Arabian Journal of Chemistry (2022) **15**, 103817

King Saud University

Arabian Journal of Chemistry

www.ksu.edu.sa
www.sciencedirect.com

ORIGINAL ARTICLE

Performance and mechanisms of NaOH and ball-milling co-modified biochar for enhanced the removal of Cd^{2+} in synthetic water: A combined experimental and DFT study

Hua Du [a], Cunxian Xi [b], Bobin Tang [b], Wenli Chen [a], Wei Deng [d], Shurui Cao [c,*], Guihua Jiang [a,d,e,*]

[a] *College of Pharmacy, Chengdu University of TCM, Sichuan 611137, China*
[b] *The Inspection Technical Center of Chongqing Customs, Chongqing 400020, China*
[c] *Forensic Identification Center, Southwest University of Political Science and Law, Chongqing 401120, China*
[d] *College of Ethnic Medicine, Chengdu University of TCM, Sichuan 611137, China*
[e] *State Key Laboratory of Southwestern Chinese Medicine Resources, Sichuan 611137, China*

Received 4 January 2022; accepted 23 February 2022
Available online 5 March 2022

KEYWORDS

Biochar;
Water treatment;
Cadmium;
Adsorption kinetics and isotherm;
Mechanism;
DFT calculation

Abstract A multifunction magnetic carbonaceous adsorbent (MBM/OH/BC) was synthesized by facile NaOH and ball-milling co-modified biochar, and applied for removing Cd^{2+} in water. The results showed MBM/OH/BC exhibited excellent adsorption capacity (183.59 mg/g for Cd^{2+}), short equilibrium time (60 min) and good reusability (the declining efficiency $<20\%$ after four adsorption and desorption cycles) compared with pristine biochar. Meanwhile, the modification mechanisms of NaOH and ball-milling to biochar were explored by a series of characterizations (XRD, SEM-EDS, BET, XPS and FTIR, et al). The results indicated the remarkable adsorption performance of MBM/OH/BC was mainly attributed to the co-modification significantly increased the specific surface area, mineral content and cation exchange capacity of biochar, thereby further improving the precipitation, cation exchange and complexation with Cd^{2+}. In addition, the results of adsorption mechanisms showed that the joint contribution proportion to the total adsorption capacity of precipitation, cation exchange and complexation was up to 90%, indicating the three

* Corresponding authors.
E-mail addresses: Caoshurui@yeah.net (S. Cao), 11469413@qq.com (G. Jiang).
Peer review under responsibility of King Saud University.

Production and hosting by Elsevier

https://doi.org/10.1016/j.arabjc.2022.103817

mechanisms were the primary adsorption mechanism. To sum up, NaOH and ball-milling co-modification was an effective strategy to increase the adsorption capacity of the pristine biochar for heavy metals from water.

1. Introduction

Various industries, including metal processing, electroplating and mining, produce a large amount of heavy metal wastewater. (Cheng, et al., 2021a; Cheng, et al., 2021b). Cadmium (Cd) is one of the most toxic heavy metals, which can accumulate in organisms and enter human organs through the food chain (Guo, et al., 2017). It would destroy the activity of the enzyme, resulting in a variety of illnesses, for example, renal dysfunction, and even life-threatening (Chen, et al., 2019; Cheng, et al., 2021a; Cheng, et al., 2022; Fu, et al., 2013; Glicklich, et al., 2020; Johri, et al., 2010). Therefore, many efforts have been made to solve the problem of heavy metals pollution, which mainly include photocatalytic degradation, oxidation, reduction, precipitation and adsorption (Chen, et al., 2019; Fu, et al., 2021; Wang, et al., 2021). Among them, adsorption has been considered the most attractive method (Chen, et al., 2021; Islam, et al., 2021; Zhou, et al., 2022). In particular, biochar is considered to be one of the most ideal adsorbents, and has aroused wide attention. It has the advantages of low-cost and environmentally-friendly performances. (Aichour, et al., 2022; Baharum, et al., 2020; Huang, et al., 2018; Li, et al., 2018; Qiu, et al., 2021; Yang, et al., 2021). Biochar is a solid product with porous, insoluble, stable, highly aromatic and carbon-rich properties, which is obtained by pyrolysis of biomass residue (straw, rice husk, sawdust, sludge, distiller's grains, kitchen waste, tea residue, etc.) under anaerobic or limited conditions. (Wang, et al., 2019; Zubair, et al., 2021). However, the adsorption performance of pristine biochar for heavy metals ions may be limited by its heterogeneity, few functional groups and low specific surface area. And most of the pristine biochar is difficult to satisfy the advantages of excellent adsorption capacity, rapid adsorption rate and simple regeneration at the same time. Therefore, to improve its adsorption capacity, adsorption rate and reusability at the same time, it has become necessary to use physical or chemical modification to modify the pristine biochar.

Chemical modification methods mainly include acid modification, alkali modification and other organic solvent modification (Ding, et al., 2016; Fernando, et al., 2021; Munera-Echeverri, et al., 2018; Tang, et al., 2021; Xu, et al., 2016; Zoroufchi Benis, et al., 2020). Among them, alkali modification can significantly increase the specific surface area of biochar, thereby improving the adsorption efficiency of pollutants (Zhou, et al., 2018; Zhou et al., 2020b). At the same time, some research has found that alkali activation biomass could significantly increase the content of minerals in biochar, for example, CO_3^{2-} and PO_4^{3-}, which could increase the precipitation with cadmium (Herath, et al., 2021). In summary, alkali modification can increase the specific surface area and mineral content of the pristine biochar at the same time, so as to improve the ability of biochar to adsorb heavy metal ions.

Ball-milling is an effective physical modification technique to obtain nanomaterials by mechanically reducing the size of particles (Xiao, et al., 2020), which can significantly improve the specific surface area, uniformity and dispersion of the material. More importantly, it also can increase the mineral content of biochar, thereby improving the adsorption capacity of pollutants. Meanwhile, the ball-milling method has the advantages of ease of operation, low cost and being environmentally friendly (Xiao, et al., 2020). Thus, ball-milling technology has been widely used to prepare various nanomaterials (Honghong Lyu, et al., 2018). Lyu et al, prepared ball-milled biochar and it was used to strengthen the adsorption capacity of Hg^{2+} and organic CH_3Hg^+ (Lyu, et al., 2020). Zhuang et al, synthesized ball-milling biochar under different conditions for efficient removal of volatile organic compounds (Zhuang, et al., 2021). Zhang et al, synthesized ball-milled biochar and it enhanced the ability to remove galaxolide (Zhang et al., 2019a). Therefore, the ball-milling method is also an effective modification method for improving the performance of biochar adsorb to heavy metal ions.

In addition, to improve the reusability of biochar materials and realize the rapid separation of pollutants from complex matrices, the magnetic properties of the materials are necessary (S. Zhang, et al., 2019). In recent years, some methods that make the adsorbent has magnetic characteristics have been reported by attaching magnetic particles to the adsorption materials, such as co-precipitation, hydrolysis and pyrolysis (Han, et al., 2015; Hu, et al., 2015; Li, et al., 2020; Zhang, et al., 2013). However, these methods still have limitations, such as, co-precipitation can cover the pore structures of the biochar, causing the active site to be decreased, and the hydrolysis and pyrolysis can cause uneven distribution of ions in biochar and require considerable energy consumption, moreover, the above methods need to use a lot of organic solvents, which may cause pollution to the environment (Li, et al., 2020; Sun, et al., 2019; Thines, et al., 2017). Compared with the above methods, the ball-milling method can fix the magnetic particles on the adsorbent through high-speed mechanical energy without adding any solvent, so as to overcome the limitations of the above methods. Therefore, ball-milling, as the green and solvent-free method, showed great promise for producing magnetic bio-nanomaterial. Meanwhile, it also can improve the adsorption performance for heavy metal ions. Such as, Wang et al, prepared magnetic Fe^0-BC material based on biochar and ion powder, which showed good magnetism (Wang, et al., 2020). Shan et al, applied the ball-milling technology to synthesize the ultra-fine magnetic BC-Fe_3O_4, which showed it easy to be separated magnetically (Shan, et al., 2016).

In conclusion, ball-milling and alkali modification can not only improve the adsorption capacity and adsorption rate of biochar for heavy metals but also improve its reusability. However, the modification mechanism is still unclear.

The overall goal of this study was to develop a novel magnetic carbon nanomaterial based on the citrus peel (Pericarpium citri reticulatae) with NaOH and ball-milling modification for

enhancing heavy metal cadmium adsorption in water, and to explain in-depth its modification mechanism adsorption mechanism. The specific objectives were as follows: (i) to prepare and characterize magnetic biochar materials (XRD, FTIR, XPS, SEM, BET, Raman and VSM); (ii) to investigate the influence of NaOH modification and ball mill modification on the adsorption performance of biochar; (iii) to study the qualitative and quantitative mechanism of MBM/OH/BC adsorbing cadmium and to compare the relative contribution of different adsorption mechanism to total adsorption capacity by a series of characterizations and batch experiments; (iv) to investigate the adsorption behavior of MBM/OH/BC by adsorption kinetics and isotherms models for better understanding of adsorption process. (v) to in-depth explore the microscopic mechanism of adsorption of heavy metal cadmium by biochar from the perspective of molecule and atom based on density functional theory.

2. Materials and methods

2.1. Reagents and solutions

The cadmium nitrate tetrahydrate ($Cd(NO)_2{\cdot}4H_2O$), HNO_3, $NaNO_3$ and NaOH were purchased from Chengdu Kelong Chemical Reagent (China). Fe_3O_4 particles were purchased from Hebei Chuancheng Metal Materials Co., Ltd. (China). Citrus peels (Pericarpium citri reticulatae) were collected from local markets (Chengdu, China). The collected waste citrus peels were dried at 60 °C and then dried citrus peels were milled to a fine powder and passed through a 125-μm sieve.

2.2. Preparation of MBM-OH-BC

(1) NaOH modification: (i) 10 g of citrus peel (Pericarpium citri reticulatae) powder was added into an Erlenmeyer flask, 20 mL of 20% NaOH was added and soaked for 3 h. (ii) An appropriate amount of water is added to the Erlenmeyer flask to wash away the excess NaOH. (iii) A small amount of 1 mol/L HCl solution was added into the Erlenmeyer flask and used to remove the redundant NaOH. (iv) The above-mixed solution was vacuum filtered and dried at 80 °C and sieved with a 125-μm sieve.

(2) Preparation of biochar (OH/BC): 6 g of NaOH modified citrus peel powder was added into the porcelain boat and pyrolyzed under different temperatures (500 °C, 600 °C, 700 °C, 800 °C) under the N_2 atmosphere. The heating program was as follows: (i) the temperature rises from 25 °C to the final temperature and maintaining it for 2 h (5 °C/min), and then cooling to room temperature in a tube furnace. The products were milled to a fine powder and named OH/BC-500, OH/BC-600, OH/BC-700 and OH/BC-800, respectively. Meanwhile, unmodified biochar was prepared using the same method, which products were named BC-500, BC-600, BC-700 and BC-800, respectively.

(3) Preparation of magnetic ball-milling biochar (MBM/OH/BC): 2 g of each biochar (OH/BC-X) and 2 g Fe_3O_4 and 200 g agate balls (diameter = 6 mm) were placed in 500 mL agate jars, then the ball mill was conducted by the ball mill machine (QM-3SP2, Nanjing University Instrument Factory, China). The speed was 500 rpm, the time was 12 h, and the rotation direction was changed every 3 h. The products were named as MBM/OH/BC-X.

2.3. Characterization of sorbents

The methods of characterization were summarized in the supplementary materials.

2.4. Batch adsorption experiments

The schematic illustration of the batch adsorption experiment was shown in Fig. S1 and was conducted as follows: (i) 5 mg sorbent was mixed with the 5 mL Cd^{2+} solutions (200 mg L^{-1}) of initial pH = 7. (ii) the mixed solutions were agitated with a constant temperature reciprocating shaker (SHA-B, Shanghai Bilang, China) at a speed of 150 rpm. (iii) The complex of adsorbent and analytes was isolated from the solution with an external strong magnet or centrifuged for 5 min (13,000 rpm). (iv) The supernatant was filtered with a 0.22 μm nylon filter. (v)The samples were analyzed by the ICP-OES with working wavelengths of 228.802 nm. The desorption experiment was conducted with 0.1 mol/L HNO_3 and deionized water for 24 h at 25 °C. The initial pH (2–7) was adjusted by adding 0.1 mol/L HNO_3 or 0.1 mol/L NaOH solution. The ionic strength of the initial Cd^{2+} solutions was adjusted with $NaNO_3$ solution. All experiments were performed 3 repetitions, and the results were described as the mean ± SD.

The adsorption capacity Q_e ($mg{\cdot}g^{-1}$) for Cd^{2+} was calculated by using equation (1):.

$$Q_e = [(C_0 - C_e) * V]/W \quad (1)$$

where C_0 ($mg{\cdot}L^{-1}$), C_e ($mg{\cdot}L^{-1}$), V (L) and W (g) are the initial Cd^{2+} concentration, the Cd^{2+} concentration at equilibrium, the volume of the Cd^{2+} solution and the amount of adsorbent, respectively.

2.4.1. Adsorption kinetic

The determination of contact time and adsorption kinetic was performed at the different time intervals for 5 h (5, 10, 30, 60, 120, 180, 240 and 300 min). The model formulas of adsorption kinetics were as follows (Du, et al., 2021; Liu, et al., 2021):.

$$Pseudo-first-order(PFO)model: Ln(Q_e - Q_t) = LnQ_e = K_1 t Ln(Q_e - Q_t) \quad (2)$$

$$Pseudo-second-order\ (PSO)\ model: t\ /\ Q_t = 1\ /\ K_2 Q_e^2 + t\ /\ Q_e \quad (3)$$

where Q_e ($mg{\cdot}g^{-1}$), Q_t ($mg{\cdot}g^{-1}$), t (min) and K_1 (min^{-1}), K_2 ($g{\cdot}mg^{-1}{\cdot}min^{-1}$) and K_i ($mg{\cdot}g^{-1}{\cdot}\ min^{1/2}$) were removal amount of Cd^{2+} at equilibrium time and t time, and adsorption time, and the corresponding rate constants, respectively.

2.4.2. Adsorption isotherm

Various adsorption isotherm models, including Langmuir, Freundlich and Dubinin-Radushkevich model, are also considered to be the basis for describing the interaction between adsorbent and adsorbate. The Langmuir isotherm model assumes that adsorption occurs on homogeneous surfaces that contain identical and equivalent sites. Freundlich isotherm model assumes that the adsorption process was mainly heterogeneous and multilayer adsorption (Du, et al., 2021). The Dubinin-Radushkevich model could be used to determine if

adsorption occurred by physical or chemical processes (Sari, et al., 2007). The adsorption isotherm experiment was performed with an initial Cd^{2+} concentration in the range from 10 − 500 mg/L (10, 50, 100, 200, 300 and 500 mg/L). The model formulas of adsorption isotherm were as follows (Romero-González, et al., 2005; Yu, et al., 2020):.

$$Langmuir\ model:\ 1\ /\ Q_e = 1\ /\ Q_m K_L C_e^2 +\ 1\ /\ Q_m \quad (4)$$

$$Freundlich\ model:\ LnQ_e = LnK_F +\ 1/n\ C_e \quad (5)$$

$$Dubinin--Radushkevich\ (D--R)\ model: LnQ_e = LnQ_m - \beta\varepsilon^2 \quad (6)$$

$$\varepsilon\ = RTLn(1 + (1/C_e)) \quad (7)$$

$$E =\ 1/(-2\beta)^{1/2} \quad (8)$$

where Q_m ($mg{\cdot}g^{-1}$) and Q_e ($mg{\cdot}g^{-1}$) are the maximum capacity and the amount of Cd^{2+} adsorbed at equilibrium, respectively; K_L ($L{\cdot}mg^{-1}$), K_F ($mg{\cdot}g^{-1}$), 1/n and C_e ($mg{\cdot}L^{-1}$) are Langmuir constant, adsorption capacity in the unit concentration, the intensity of adsorption and the equilibrium concentration, respectively. β, ε and E (kJ/mol) are activity coefficient, the Polanyi potential and the mean adsorption energy, respectively.

2.5. Quantitative adsorption mechanisms

The total contributions of mechanisms (Q_T) for Cd^{2+} on biochar include chemical adsorption mechanism (Q_{chem}) and physical adsorption mechanism (Q_{phy}). The chemical adsorption mechanism (Q_{chem}) mainly is composed of co-precipitation (Q_{pre}), cation exchange (Q_{exc}), complexation (Q_{com}) and Cd^{2+}-π interaction ($Q_{c\pi}$). Those mechanisms could be determined according to previous methods (Chen, et al., 2020; Gao, et al., 2019; Huang, et al., 2020; Li, et al., 2018; Liu, et al., 2020; Zhang et al., 2021b).

(i) The physical adsorption (Q_{phy}) was considered to be the content of desorbed Cd^{2+} from deionized water, and the chemical adsorption mechanism (Q_{chem}) was described that the total adsorption mechanism (Q_T) removes the physical adsorption mechanism, which was as follows:.

$$Q_{chem} =\ Q_T - Q_{phy} \quad (9)$$

(ii) The co-precipitation (Q_{pre}) mainly originates from minerals, thus it was calculated based on the difference of the adsorption capacity for Cd^{2+} by the adsorbent between before and after demineralization. The demineralized method is as following: the biochar after adsorbing Cd^{2+} was washed three times with 1 mol/L HNO_3 solution, then washed with deionized water to a constant pH value.

$$Q_{pre} = Q_{chem} - Q_{de} *\ Y \quad (10)$$

where Q_{de} ($mg{\cdot}g^{-1}$) is the adsorption ability of biochar to Cd^{2+} after demineralization. Y is the yield of demineralized biochar from the original biochar.

(iii) The cation exchange (Q_{exc}) is equal to the amounts of cations (K^+, Na^+, Ca^{2+} and Mg^{2+}) that are released into the solution after biochar adsorbed Cd^{2+}.

$$Q_{exc} = Q_k + Q_{Na} + Q_{Ca} + Q_{Mg} \quad (11)$$

where Q_k, Q_{Na}, Q_{Ca} and Q_{Mg} ($mg{\cdot}g^{-1}$) are the amount of K^+, Na^+, Ca^{2+} and Mg^{2+}, respectively.

(iv) The complexation (Q_{com}) was originated from the oxygen-containing functional groups, and the decrease in pH before and after biochar adsorption of cadmium is only due to the complexation between the oxygen-containing functional groups in the demineralized biochar and Cd2+. The process of demineralization could not change the surface oxygen-containing functional groups of biochar. Thus, the complexation (Q_{com}) could be calculated as follows:.

$$Q_{com} = Q_{pH} *\ Y \quad (12)$$

where Q_{pH} ($mg{\cdot}g^{-1}$) is the adsorbed Cd^{2+} by complexation with oxygen-containing function groups on demineralized biochar.

(v) Cd^{2+}-π interaction ($Q_{c\pi}$) was calculated by subtracting other chemical adsorption mechanisms from the total chemical adsorption mechanism.

$$Q_{c\pi} =\ Q_{chem} - Q_{com} - Q_{pre} - Q_{exc} \quad (13)$$

2.6. DFT calculation method

The binding energy between Cd^{2+} and biochar was calculated by the Material Studio (MS) software based on Dmol3 package. The biochar model was represented by the structure of 7 aromatic rings containing oxygen functional groups, and the edge of aromatic rings is compensated by H atoms. The binding energy was calculated by $E_{ad} = E_t - (E_{sor} + E_{cd})$, where E_t is total energy of sorbent after adsorption of Cd^{2+}. E_{sor} is the energy of sorbent. E_{cd} is the energy of Cd^{2+}. The electrostatic potential (ESP) was performed based on the Material Studio (MS) software based on Dmol3 package (K. Zhou, et al., 2020).

3. Result and discussion

3.1. Performance of Cd^{2+} adsorption by MBM/OH/BC

3.1.1. Effect of pH

pH is a key factor that affects the adsorption efficiency of biochar for heavy metal ions. It not only affects the ionization degree of heavy metal ions in the solution but also determines the charge form (positive or negative) on the surface of the adsorbent (P. Zhang, et al., 2021). Thus, the effect of different initial solution pH values on the adsorption efficiency was studied. At first, to prevent the precipitation problem of Cd^{2+} and ensure the solubility of Cd^{2+}, the metal speciation of cadmium in different pH (2–14) aqueous phases was calculated by Visual MINTEQ ver.3.1 modeling program (Zhu, et al., 2020). The modeling result showed that no precipitation ($Cd(OH)_x$) was formed when the pH of the initial solution was less than 7, and the $Cd(OH)_x$ would be generated when the pH was greater than 7 (Fig. 1a). Thus, the initial solution pH from 2 to 7 was investigated in the current study. According to Fig. 1b, it could be found that the pH had a significant effect on the cadmium adsorption capacity of MBM/OH/BC. The adsorption capacity of cadmium increased with the increase of pH of the solution, and the maximum adsorption capacity was observed at pH = 7. The above experimental results could be explained by the fact: (i) At the low pH, the H^+ concentra-

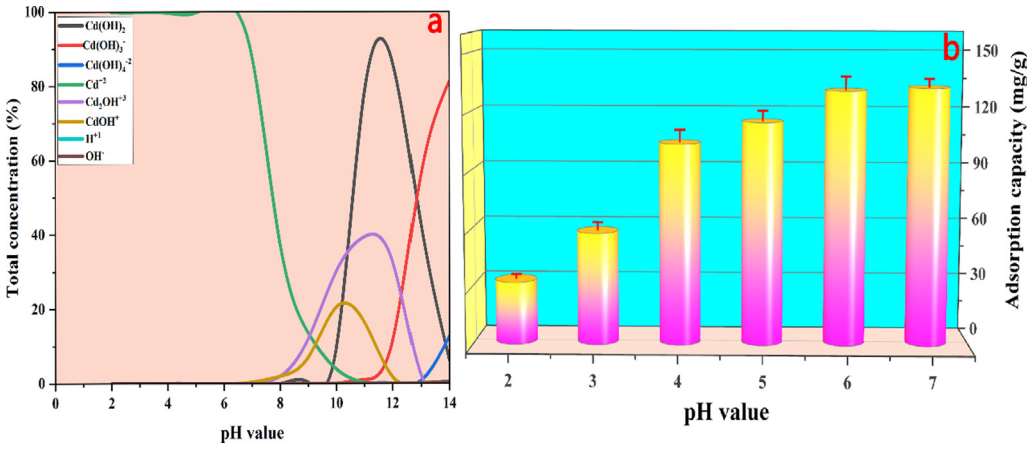

Fig. 1 (a) The speciation of cadmium in the aqueous phase at different pH. (b) The effect of different initial solution pH on the Cd^{2+} adsorption capacity.

tion was high and it might compete for the adsorption sites with metal cation (M^+), thereby resulting in the decrease of adsorption capacity for Cd^{2+}. And the concentration of H^+ gradually decreased with the increasing pH, and the competition between H^+ and Cd^{2+} also weakened, thus increasing the adsorption capacity for Cd^{2+} (P. Zhang, et al., 2021). (ii) At higher H^+ concentrations, H^+ might react with minerals (CO_3^{2-}) of the biochar material, thereby reducing the mineral content and further reducing the precipitation of Cd^{2+}, thus the adsorption capacity was weakened (Liu, et al., 2020). (iii) According to Fig. S2, it could be found that the pH_{pzc} of MBM/OH/BC was 10.52. When the pH of the solution is less than pH_{pzc}, the MBM/OH/BC might be protonated, which may hinder the adsorption of Cd^{2+} duo to electrostatic repulsion (Gao, et al., 2019). In this study, pH = 7 was the closest to pH_{pzc}, thus the electrostatic repulsion was the weakest at pH = 7, and the best adsorption capacity was found when the initial concentration was pH = 7. In summary, pH = 7 was selected as the optimum condition.

3.1.2. Contact time and adsorption kinetic

To determine the equilibrium time and to compare the adsorption rate of biochar before and after modification (MBM/OH/BC and BC), the contact time from 5 to 300 min was investigated. According to Fig. 2, it could be found that the adsorption rate after modification (MBM/OH/BC) was twice that before modification (BC). The equilibrium time of MBM/OH/BC and BC was approximately 60 min and 120 min, respectively, which showed that the adsorption rate of biochar could be significantly improved by NaOH and ball-milling modification. Meanwhile, to ensure the process reached equilibrium completely, the subsequent experiment was carried out using 60 min as contact time.

In addition, to deeply study the relationship between adsorbent, adsorbate and adsorption time and to understand the adsorption process of heavy metal ions on biochar (Du, et al., 2021), the PFO kinetic model and PSO kinetic model were utilized to fit the data of batch adsorption experiments. The kinetic curve and fitting parameters were shown in Fig. 3a and Table 1. According to Fig. 3a, it could be found that the adsorption process was divided into three steps, which included the fast adsorption, slow adsorption and dynamic equilibrium stage. It could be interpreted as: at the initial stage, a large number of active sites were not occupied, so Cd^{2+} was easily captured by the adsorbent through electrostatic attraction. As the contact time went by, the most of adsorption sites and pore spaces were occupied, thus the adsorption rate of Cd^{2+} was decreased. Finally, the electrostatic repulsion between the adsorbed Cd^{2+} and the Cd^{2+} in the solution prevented the subsequent adsorption (Hosseini, et al., 2021).

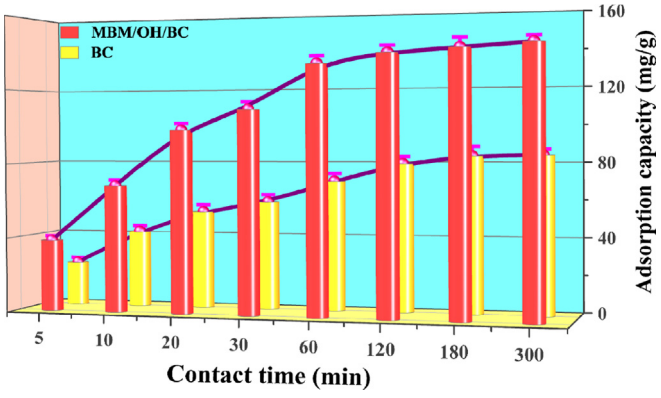

Fig. 2 The effect of different contact time on the Cd^{2+} adsorption capacity.

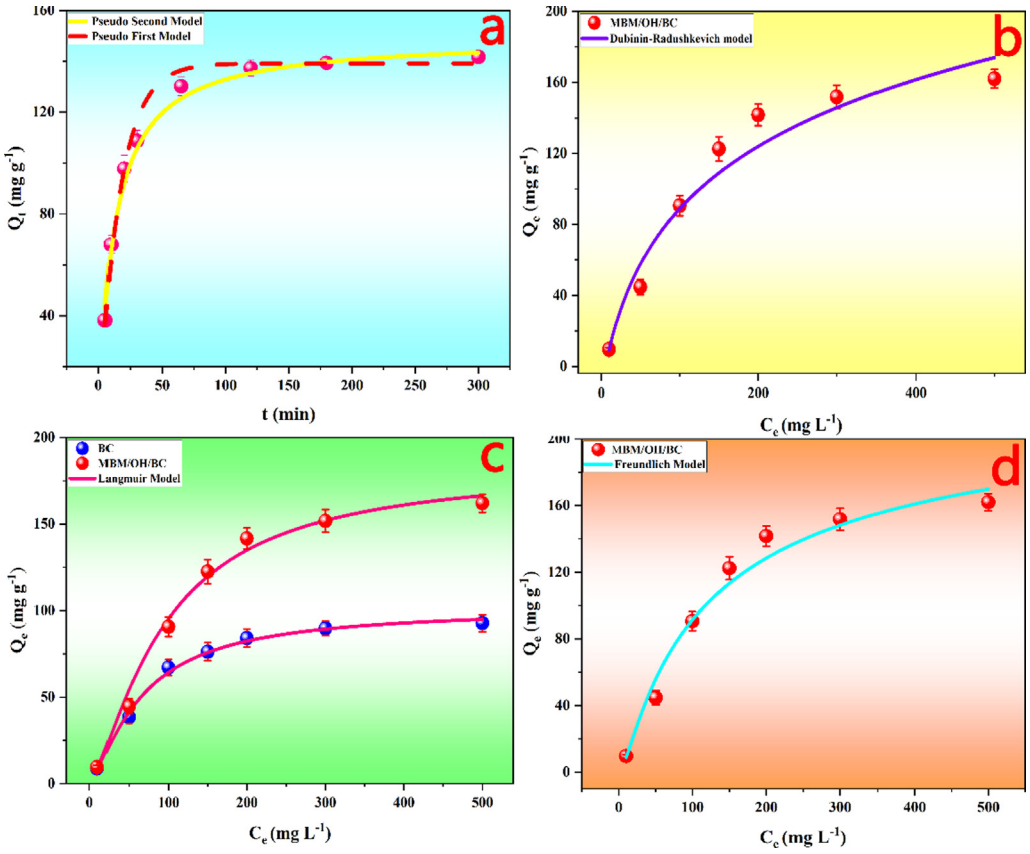

Fig. 3 (a) The fitting curves of the pseudo-first-order kinetic model and pseudo-second-order kinetic model. The fitting curves of Dubinin–Radushkevich (b), Langmuir (c) and Freundlich (d) adsorption isotherms model.

Table 1 The parameters of the pseudo-first-order and pseudo-second-order adsorption kinetic models for the adsorption of Cd^{2+} onto MBM/OH/BC.

	Q_e (exp)	Pseudo-first-order kinetic model			Pseudo-second order kinetic model		
		Q_e	K_1	R^2	Q_e	K_2	R^2
Cd^{2+}	141.34	138.63	0.1361	0.992	142.43	0.0606	0.994

According to Table 1, it could be found that the R^2 value of the PSO kinetic model was closer to 1 than the PFO kinetic model, which were 0.994 and 0.992, respectively. And the Q_e value calculated by the PSO model was consistent with the experimental Q_e value. The results indicated the adsorption process of Cd^{2+} on MBM/OH/BC was more suitable to be described by PSO and Cd^{2+} adsorption by MBM/OH/BC were mainly controlled by chemical adsorption (Huang, et al., 2018; P. Zhang, et al., 2021), for example, precipitation, cation exchange and complexation, which was consistent with previous studies (Gao, et al., 2019; Huang, et al., 2020; Yu, et al., 2018).

3.1.3. Adsorption isotherm studies

The fitting curves of the three models (Langmuir, Freundlich and Dubinin-Radushkevich model) were shown in Fig. 3b-d,

Table 2 The Parameters of the Freundlich, D-R isotherm and Langmuir model for the adsorption of Cd^{2+} onto MBM/OH/BC.

	Freundlich isotherm model			Langmuir isotherm model			Dubinin–Radushkevich (D–R) model		
	K_F (mg g^{-1})	n	R^2	Q_m (mg g^{-1})	K_L (L g^{-1})	R^2	β (mol^2/J^2)	E (kJ/mol)	R^2
Cd^{2+}	0.0215	4.032	0.997	183.59	0.0732	0.992	-0.003.98	11.21	0.996

and the constants and coefficients were listed in Table 2. The results showed the Freundlich isotherm model (R^2 = 0.997) had a better fitting effect than the Langmuir isotherm model (R^2 = 0.992), indicating the adsorption process of Cd^{2+} on MBM/OH/BC was heterogeneous and multilayer adsorption. Meanwhile, the 1/n < 0.5 showed that the adsorption characteristics of Cd^{2+} on MBM/OH/BC were ideal (P. Zhang, et al., 2021). According to the result of the Langmuir isotherm model (Fig. 3c and Table 2), it could be clearly observed that the adsorption capacity of biochar modified by NaOH and ball-milling (MBM/OH/BC) was significantly improved, and its maximum adsorption capacity could be as high as 183.59 mg/g, which was almost twice that of unmodified biochar (BC, 101.51 mg/g), which proved that the adsorption capacity of biochar could be significantly improved by NaOH and ball-milling modification. In addition, according to the result of Dubinin-Radushkevich model fitting, the average adsorption energy (E) was 11.21 kJ/mol. Generally, if average adsorption energy (E) is less than 8 kJ/mol, the adsorption process mainly follows physical adsorption, on the contrary, if average adsorption energy (E) is greater than 8 kJ/mol, the adsorption process mainly follows chemical ion-exchange. Thus, the results of Dubinin-Radushkevich model fitting (E > 8 kJ/mol) further proved that the adsorption of Cd^{2+} on MBM/OH/BC was mainly a chemical adsorption process (Romero-González, et al., 2005; Sari, et al., 2007).

3.2. Qualitative and quantitative adsorption mechanisms

3.2.1. Precipitation

The adsorption mechanism of MBM/OH/BC for heavy metals mainly includes physical adsorption, cation exchange, precipitation, complexation and coordination between the metal ion and π electrons, and the schematic diagram was shown in Fig. 4. The precipitation effect of biochar originated from the effect of minerals, for example, CO_3^{2-} and PO_4^{3-}. By comparing the SEM images before and after MBM/OH/BC adsorption of Cd^{2+} (Fig. 5c, d), it could be clearly found that many white granular crystals were attached to the surface of MBM/OH/BC, and the white crystals were considered to be insoluble mineral cadmium precipitates. Then, the XRD spectra of the MBM/OH/BC before and after adsorption were obtained to further determine the types of mineral cadmium precipitates. Evidently, the new peak could be found in the XRD spectra of MBM/OH/BC after Cd^{2+} adsorption (Fig. S3). The new peaks were identified as $CdCO_3$ and $Cd_3(PO_4)_2$, which further confirmed that the precipitation effect between minerals and Cd^{2+} played a vital role in the adsorption process. In addition, according to the FTIR spectra (Fig. 6b), it could be found that the peak at 1085 cm^{-1} was shift to 1067 cm^{-1} after MBM/OH/BC adsorbed Cd^{2+}, the peak (1085 cm^{-1}) was correspond to the PO_4^{3-}, which indicated that the cadmium phosphate ($Cd_3(PO_4)_2$) precipitation might be formed (Huang, et al., 2020), and the peak at 1497 cm^{-1} was shift to 1477 cm^{-1}, corresponding to the CO_3^{2-}, indicating that the cadmium carbonate (Cd_3CO_3) might be formed (Huang, et al., 2018; Huang, et al., 2020). Meanwhile, by comparing the XPS spectra of MBM/OH/BC after Cd^{2+} adsorption with the original one (Fig. 7a, d), the new peaks could be found, which showed that there were a great number of Cd^{2+} on the surface of the MBM/OH/BC, among them, the binding energy of 406–410 eV assigned to $CdCO_3$ and Cd-O. Those results further proved that the precipitation of minerals was an important mechanism for MBM/OH/BC to adsorb Cd^{2+}.

3.2.2. Cation ion exchange

A large number of metal ions (K^+, Na^+, Ca^{2+} and Mg^{2+}) could be retained in MBM/OH/BC through electrostatic interaction with negative charge sites (Huang, et al., 2020). During the process of MBM/OH/BC adsorbing Cd^{2+}, the Cd^{2+} might be exchanged with the metal ions that were retained in MBM/OH/BC (K^+, Na^+, Ca^{2+} and Mg^{2+}), thereby adsorbing on MBM/OH/BC. Therefore, cation ion (K^+, Na^+, Ca^{2+} and Mg^{2+}) exchange was considered a critical mechanism for Cd^{2+} adsorption onto MBM/OH/BC. In the current study, it could be found that 26.7 mg/g (Q_e) of metal ions (K^+, Na^+, Ca^{2+} and Mg^{2+}) were released into the solution during

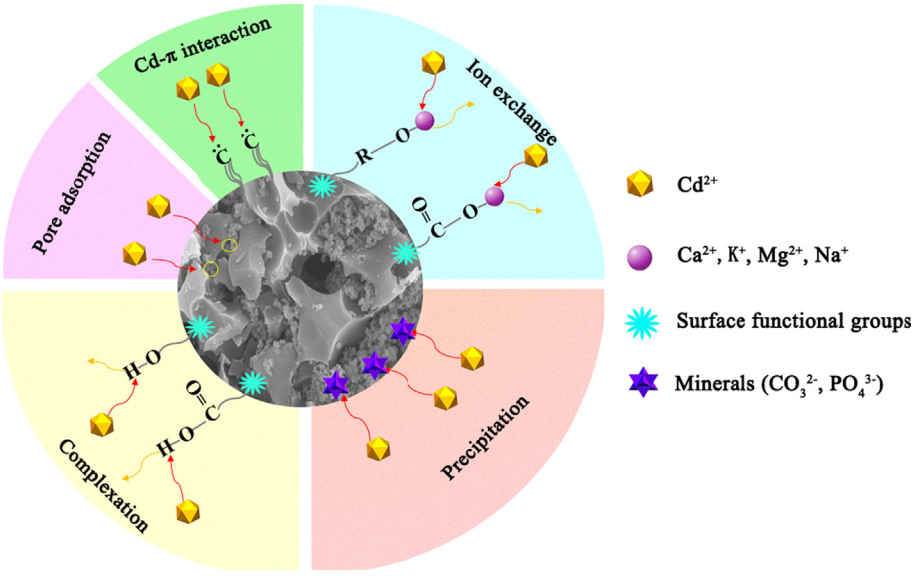

Fig. 4 The schematic diagram of the possible adsorption mechanism of Cd^{2+} on MBM/OH/BC.

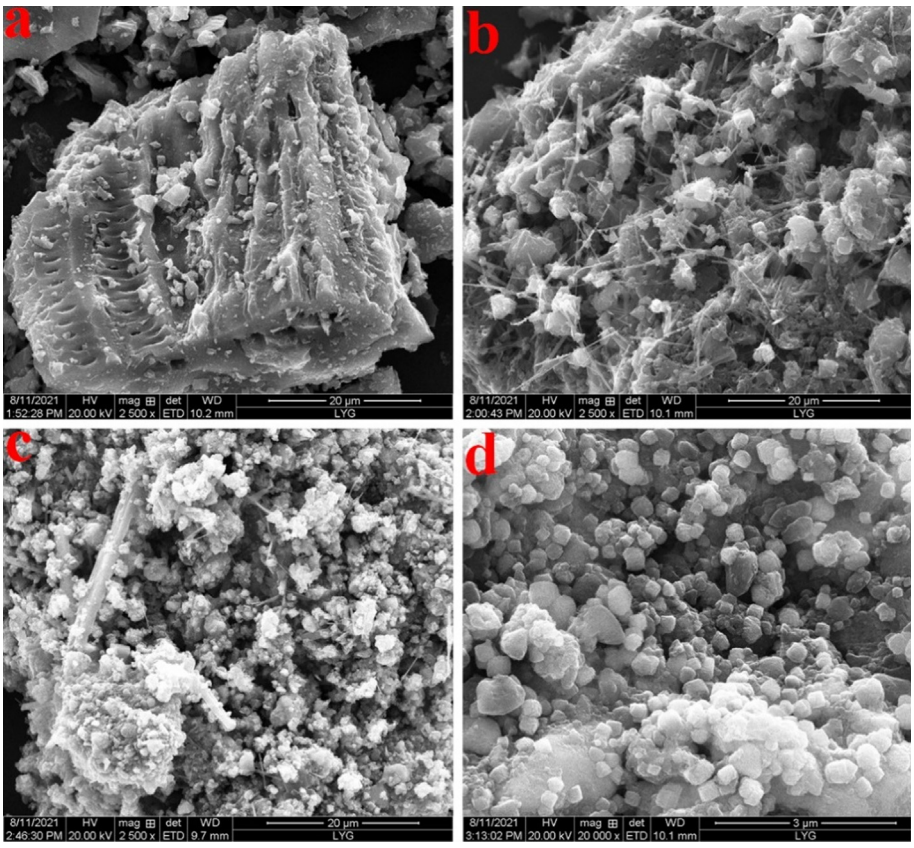

Fig. 5 The SEM images of BC (a), OH/BC (b) and MBM/OH/BC (c). (d) The SEM images of MBM/OH/BC after Cd^{2+} adsorption.

the adsorption process (Fig. 8), which was equal to the amount of cadmium adsorbed on the MBM/OH/BC (Huang, et al., 2020). It preliminarily proved that cation exchange participated in the adsorption process of Cd^{2+} in solution. In addition, according to the SEM-EDS spectra (Fig. 9c,d), it could be observed clearly that the content of K^+, Na^+, Ca^{2+} and Mg^{2+} was significantly reduced after Cd^{2+} adsorption, which further confirmed that the cation ion exchange with metal ions had occurred during the adsorption of Cd^{2+}. Therefore, the metal cations exchange was one of the indispensable mechanisms of Cd^{2+} adsorption by MBM/OH/BC.

3.2.3. Coordination

The coordination between metal ions and π electrons was also considered to be a possible adsorption mechanism. The aromatic ring and basic functional groups on the surface of biochar were electron-rich, which could provide π electrons to coordinate with heavy metal ions (Huang, et al., 2020). In

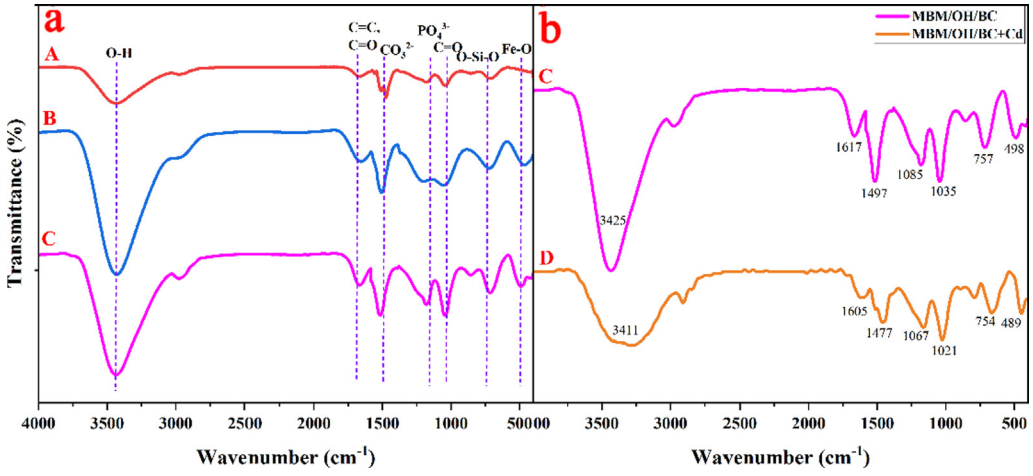

Fig. 6 (a) The FTIR spectra of BC (A), OH/BC (B) and MBM/OH/BC (C). (b) The FTIR spectra of MBM/OH/BC before and after Cd^{2+} adsorption.

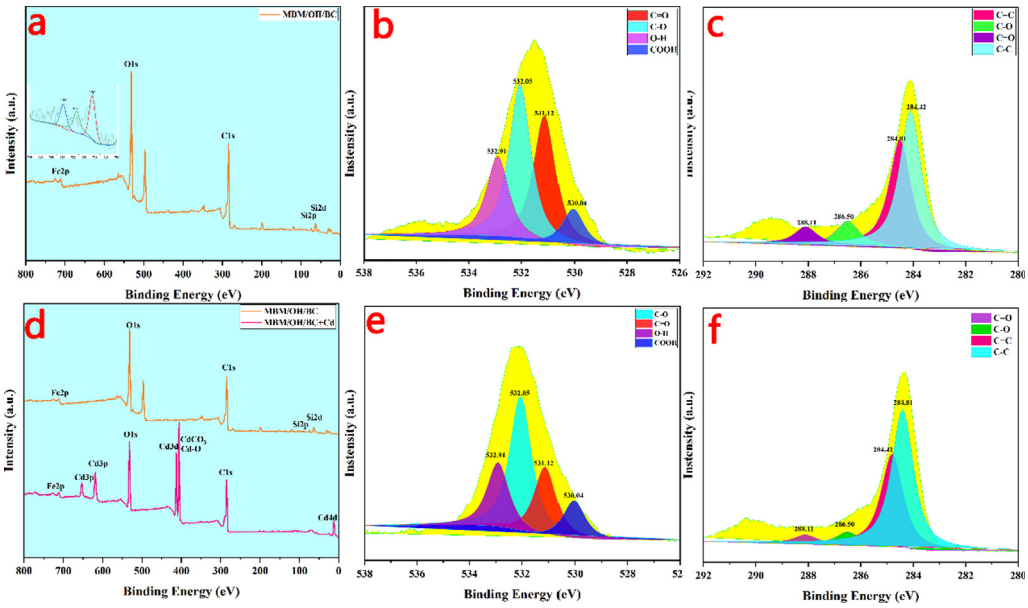

Fig. 7 The XPS scanning spectra of MBM/OH/BC before (a, b and c) and after (d, e and f) Cd^{2+} adsorption. C1s (c, f) and O1s (b, e).

the current study, FTIR spectra showed that the C = C stretching peaks of MBM/OH/BC shifted from 1617 cm^{-1} to 1605 cm^{-1}, which indicated the coordination of Cd^{2+} and π electrons might contribute to Cd^{2+} adsorption (Fig. 6b) (Gao, et al., 2019). Meanwhile, according to the Raman spectra (Fig. S4), it could be found that the peak shifted from 1359 cm^{-1} to 1374 cm^{-1} and from 1619 cm^{-1} to 1634 cm^{-1}, which might be explained as the coordination between the π electrons of the aromatic ring and the Cd^{2+} caused the redshift of the peak, which further proved that Cd^{2+} - π interaction was one of the mechanism of Cd^{2+} adsorption by MBM/OH/BC.

3.2.4. Complexation

FTIR and XPS were used to determine the changes in the surface functional groups of MBM/OH/BC before and after Cd^{2+} adsorption. According to the FTIR spectra (Fig. 6b), after Cd^{2+} adsorption, it could be found that the dominant peak at 3425 cm^{-1} (assigned to –OH) was obviously weakened, and the peak at 1617 cm^{-1} (assigned to C = O) was also significantly weakened and shifted from 1617 cm^{-1} to 1605 cm^{-1}. Those findings confirmed that the complexation of functional groups including hydroxyl and carboxyl was involved in Cd^{2+} adsorption (Liu, et al., 2020). Meanwhile, the results of XPS showed that the C1s and O1s spectra of MBM/OH/BC before and after adsorption have obviously changed (Fig. 7). After Cd^{2+} adsorption, the peak area of C-O of C1s was reduced from 9.3% to 5.4%, and the peak area of C = O was reduced from 7.2% to 4.8%. Similarly, after Cd^{2+} adsorption, the peak area of C-O and C=O of O1s spectra also reduced from 43.8% and 29.6.8% to 31.9% and 16.1%, respectively. The results further proved that the complexation between functional groups (C=O, C-O) and Cd^{2+} is involved during the adsorption process (Liu, et al., 2020). Therefore, the complexation was also considered as a critical mechanism of Cd^{2+} adsorption by MBM/OH/BC.

3.2.5. Quantitative mechanism distribution

In addition, in order to further analyze the contribution of several adsorption mechanisms to the total adsorption capacity, their respective adsorption capacity and contribution rate were quantitatively calculated. The results were shown in Fig. 8. It could be found that the precipitation, cation exchange and complexation was the main adsorption mechanism for MBM/OH/BC to adsorb Cd^{2+}, which was consistent with previous studies (Huang, et al., 2018). The contribution rates of

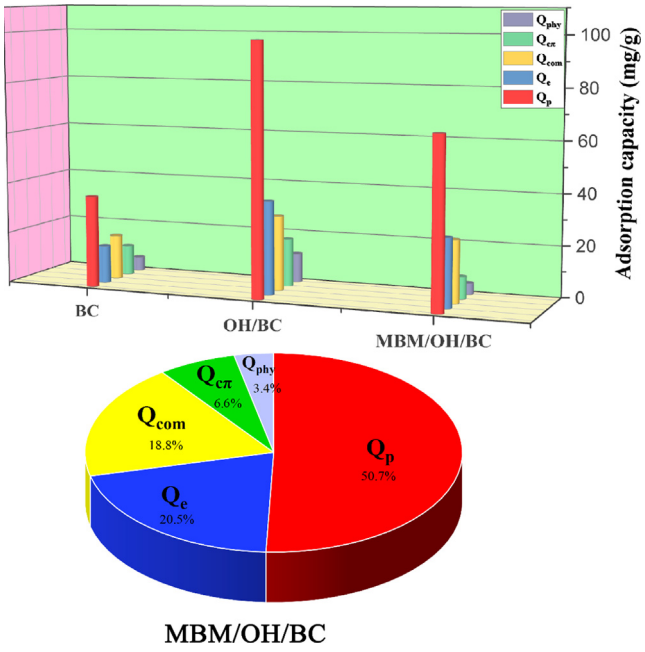

Fig. 8 The adsorption capacity of Cd^{2+} from the different mechanisms on the three biochar. The contribution rate of different mechanisms to total adsorption capacity.

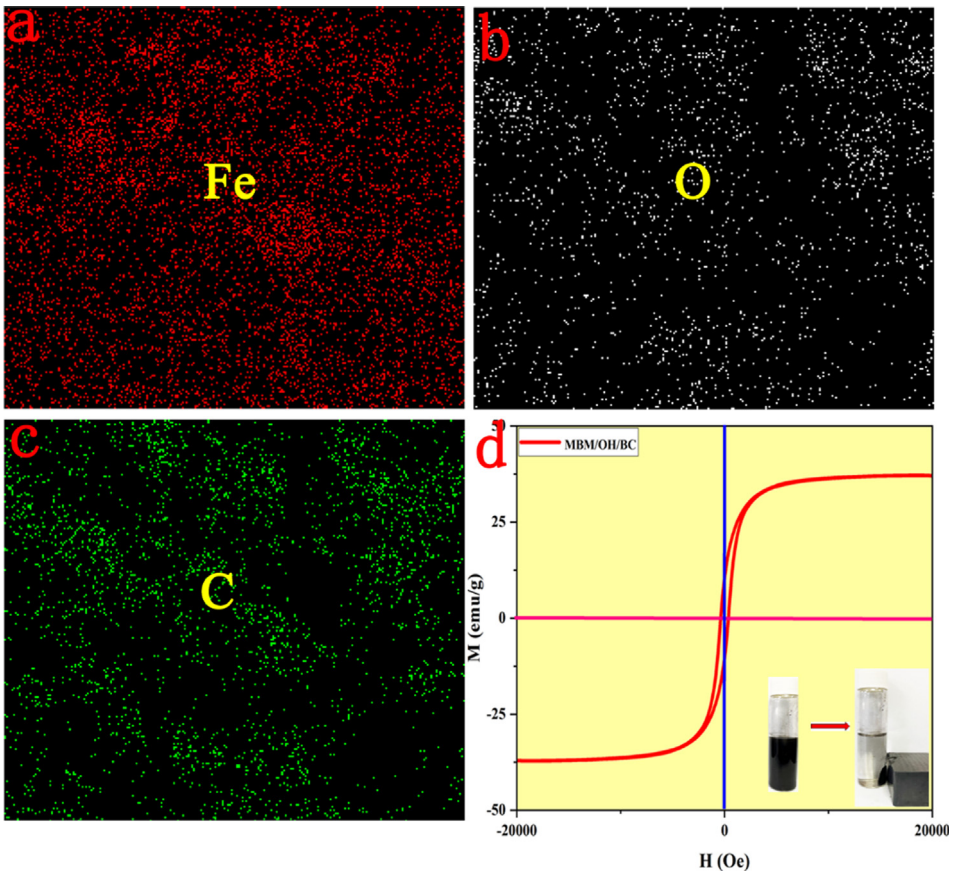

Fig. 9 (a-c) The elements mapping of MBM/OH/BC. (d) The VSM curves of MBM/OH/BC, and the right inset showed the absorbent dispersed in sample solution and the magnetic separation.

the precipitation, cation exchange and complexation were 50.7%, 20.5% and 18.8% respectively, which explained 90% of the total adsorption mechanism, however, the physical adsorption and interaction of metal ion and π electrons only explained 10% of the total adsorption mechanism, which showed that the two mechanisms were minor importance (Huang, et al., 2020). More importantly, by comparing the quantitative adsorption mechanism distribution of modified and unmodified biochar, it could be observed that the precipitation, cation exchange and complexation of modified biochar (MBM/OH/BC) were significantly increased, and the precipitation, cation exchange and complexation had increased from 35.9 mg/g, 14.7 mg/g and 17.7 mg/g to 65.8 mg/g, 26.7 mg/g and 24.4 mg/g, respectively. It explained the reason why NaOH and ball-milling modification could improve the adsorption capacity of biochar was that it increased the precipitation, cation exchange and complexation of biochar.

3.3. DFT calculation

In order to better explore the interaction mechanism between biochar adsorbent and Cd^{2+} at the molecular or atomic level, the quantum chemistry calculation based on the density functional theory (DFT) was applied. Combined with the results of XPS and FTIR, it could be found that the oxygen-containing functional group on the biochar mainly included hydroxyl, carbonyl and carboxyl (OH, C = O and COOH). Thus, the four computational models with various oxygen-containing functional groups modified graphene structure was constructed, and the adsorption energy was calculated. The optimized geometries and adsorption energy were shown in Fig. 10. According to Fig. 10, the binding energy of COOH-graphene, C = O-graphene OH-graphene, and pure graphene were −123.45 kJ/mol, −121.56 kJ/mol, −126.17 kJ/mol and −116.93 kJ/mol, respectively. The greater the absolute value of the binding energy, the greater the binding energy of the adsorbent and Cd^{2+} (Feng, et al., 2021). The results showed that the binding energy of graphene modified with oxygen-containing functional groups was significantly greater than that of pure graphene. The significant increase in adsorption energy could be attributed to the Lewis acid-base interaction between oxygen-containing functional groups and Cd^{2+}. Meanwhile, it further proved that the adsorption ability between biochar and Cd^{2+} could be strengthened by improving the oxygen-containing functional groups in biochar.

In addition, to further predict and explore reactive sites between MBM/OH/BC and Cd^{2+}, the electrostatic potential (ESP) analysis was performed. The metal cation was closer to the surface with the negative ESP, which indicated it was more likely to be the active site for electrophilic reactions. ESP distribution was usually considered on Van der Waals (vdW) surface. Under the default color method (blue-white-red, BWR), the blue *iso*-surface corresponded to negative ESP, and the bluer the color, the lower the ESP (Zhang

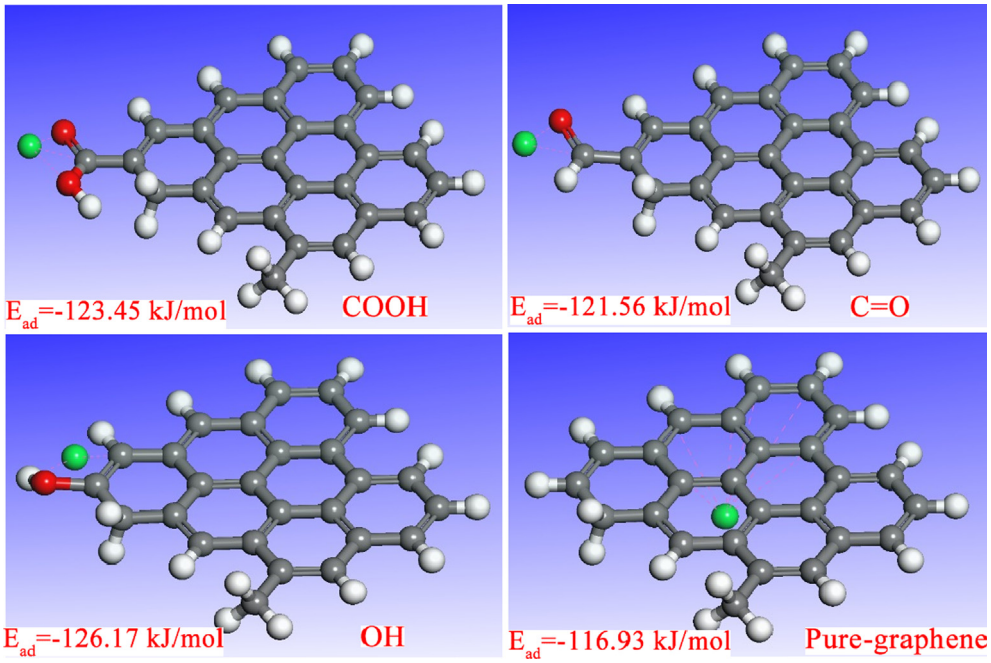

Fig. 10 The optimized geometric structures of Cd^{2+} on biochar adsorbent (COOH-graphene, C = O-graphene, OH– graphene and pure-graphene).

et al., 2021a). In the current study, the ESP *iso*-surface maps of the four computational models were depicted in Fig. 11. It could be obviously seen that the blue *iso*-surface was mainly distributed near oxygen-containing functional groups, indicating the oxygen-containing functional groups on the surface were the active sites that mainly react with Cd^{2+}. Thus, it fur-

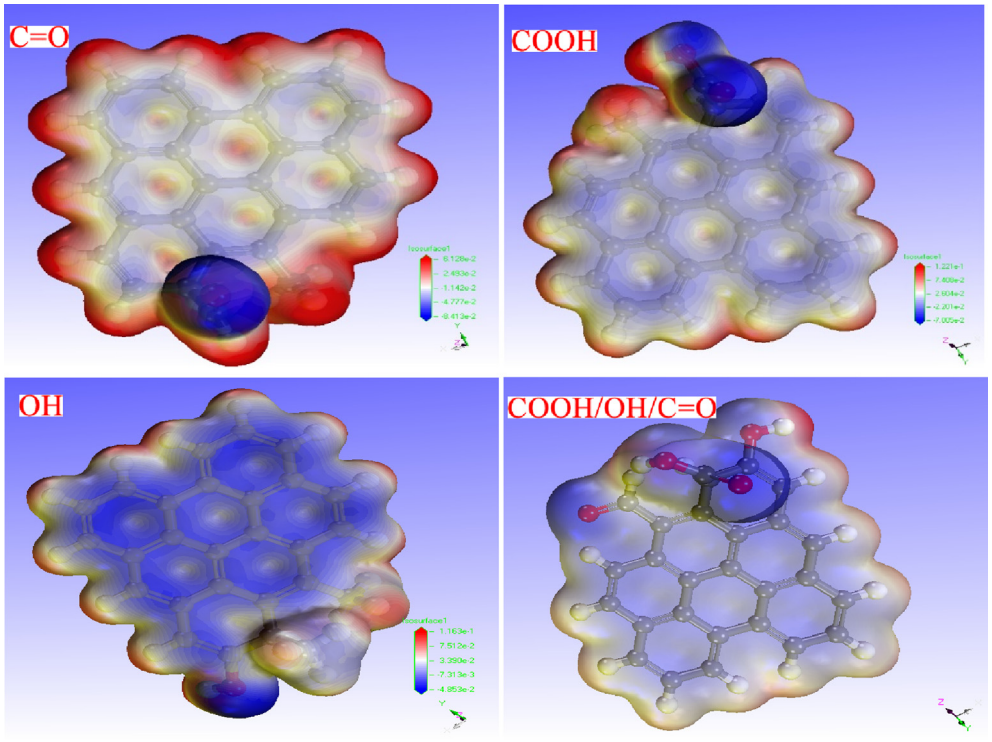

Fig. 11 The ESP iso-surface map of biochar adsorbent (COOH-graphene, C = O-graphene, OH- graphene and COOH/OH/C = O-graphene).

Table 3 The main physicochemical characteristics of BC, OH/BC and MBM/OH/BC.

Sample	Ions content (mg/g)					
	K^+	Na^+	Ca^{2+}	Mg^{2+}	CO_3^{2-}	PO_4^{3-}
BC	8.23	2.35	2.76	2.21	2.26	4.03
OH/BC	9.32	16.32	2.12	2.12	24.57	6.43
MBM/OH/BC	6.25	10.51	2.97	2.56	16.43	5.35

ther confirmed that increasing the oxygen-containing functional group content in biochar could enhance the adsorption capacity of biochar for Cd^{2+}.

3.4. Modification mechanisms of NaOH and ball-milling to biochar

Pyrolysis temperature had a significant impact on the structure and chemical composition of biochar and it was a key factor that determines the adsorption efficiency of biochar to Cd^{2+}. Thus, to obtain the best adsorption efficiency, the different pyrolysis temperature (500, 600, 700 and 800 ℃) was investigated. According to Fig. S5, it could be found that the adsorption efficiency was the highest when the pyrolysis temperature was 700℃, which could be explained that the increase of the specific surface area and mineral content of biochar as the temperature increases, facilitating the adsorption of heavy metal ions. Therefore, the 700 ℃ was selected as the optimal pyrolysis temperature. Meanwhile, it could be clearly seen that the adsorption capacity was significantly increased after NaOH modification (Fig. S5a), and the adsorption capacity of OH/BC (189.3 mg/g) was more than twice that of BC (85.2 mg/g). And after further ball-milling, the adsorption capacity was further improved. In Fig. S5b, the adsorption capacity of the MBM/OH/BC was 133.1 mg/g. In fact, the biochar adsorbent content in MBM/OH/BC only occupied 50%, and the other 50% was Fe_3O_4. Therefore, the actual adsorption capacity of MBM/OH/BC could reach close to 266.2 mg/g. In summary, the NaOH and ball-milling modification could improve the adsorption capacity of biochar for Cd^{2+}.

In order to further explore the effect of NaOH and ball-milling co-modification on the physical and chemical properties of biochar, and to explain the reason why NaOH and ball-milling co-modification could improve the adsorption efficiency of biochar to Cd^{2+}, the modified and unmodified biochar (BC, OH/BC and MBM/OH/BC) were characterized by a series of characterization methods (SEM-EDS, FTIR, BET and XPS, etc.).

3.4.1. NaOH and ball-milling modification effect on physicochemical properties

The physicochemical properties of BC, OH/BC and MBM/OH/BC were shown in Table 3. According to Table 3, it could be observed clearly that the contents of Na^+ was significantly increased after NaOH and ball-milling modification. This might be interpreted as the chemical reaction between NaOH and functional groups of the biomass to produce R-COONa, R-ONa or Na_2CO_3, which remained in the biomass (Huang, et al., 2020). The above results were consistent with the results of SEM-EDS (Fig. 12). The results showed that the percentage of K, Na, Ca and Mg elements in the modified biochar have increased significantly. It was conducive to improving the cation exchange with heavy metal ions, thereby enhancing the removal capacity of biochar for heavy metal ions. Meanwhile, it was worth noting that the content of CO_3^{2-} and PO_4^{3-} in the modified biochar were also significantly higher than the pristine biochar (Table 3), which could greatly improve the precipitation of heavy metal ions, and further increase the ability of biochar to remove heavy metal ions. The results were consistent with the results of the FTIR analysis (Fig. 6a). After the modification, the peak intensity corresponding to CO_3^{2-} and PO_4^{3-} increased significantly.

3.4.2. NaOH and ball-milling modification effect on the surface functional groups

The surface functional groups and chemical composition were investigated through FTIR and XPS. The results were shown in Fig. 6 and Fig. 7. In the FTIR spectra (Fig. 6a), the stretching vibration peak at 3425 cm^{-1} was contributed to –OH bonds; the peak at 1617 cm^{-1} corresponds to the C=C and C=O stretching vibration (Li, et al., 2020; K. Zhou, et al., 2020), which indicated that there were lots of oxygen-containing functional groups in biochar materials. Meanwhile, it was worth noting that the peak intensity of the oxygen-containing functional groups has increased after NaOH and ball-milling modification, which suggested that the NaOH modification might have introduced additional oxygen-containing functional groups and the ball-milling modification might expose the unsaturated bonds (Lyu et al., 2018a; 2018b). This was beneficial to improve the complexation between oxygen-containing functional groups and heavy metal ions and further enhance the ability to remove heavy metal ions. In addition, in the XPS survey scans of MBM/OH/BC (Fig. 7-a-c), the peak at around 284 eV, 532 eV and 700 eV corresponding to the C1s, O1s and Fe2p core level, respectively. The C1s could be deconvoluted into four sub-peaks, which include C=C (284.8 eV), C-C (284.4 eV), C=O (288.1 eV) and C-O (286.5 eV) (K. Zhou, et al., 2020). The O1s could be deconvoluted into four sub-peaks, which include O-H (532.9 eV), C=O (531.1 eV), C-O (532.1 eV) and COOH (530.1 eV) (Li, et al., 2020; K. Zhou, et al., 2020). To sum up, the above XPS results proved that there were a large number of oxygen-containing functional groups in MBM/OH/BC, which could be complex with heavy metal ions. The binding energy peaks at 724.4 eV and 718.2.4/733.3 eV in the Fe2p spectrum of MBM/OH/BC represented the existence of Fe $2p_{1/2}$ and Fe $2p_{3/2}$, which indicated the occurrence of magnetic Fe_3O_4 in MBM/OH/BC (Du, et al., 2021).

3.4.3. NaOH and ball-milling modification effect on morphologies and structures

SEM was applied to study the surface morphologies and structures of BC, OH/BC and MBM/OH/BC. The results were shown in Fig. 5. According to Fig. 5a, b, it could be found that

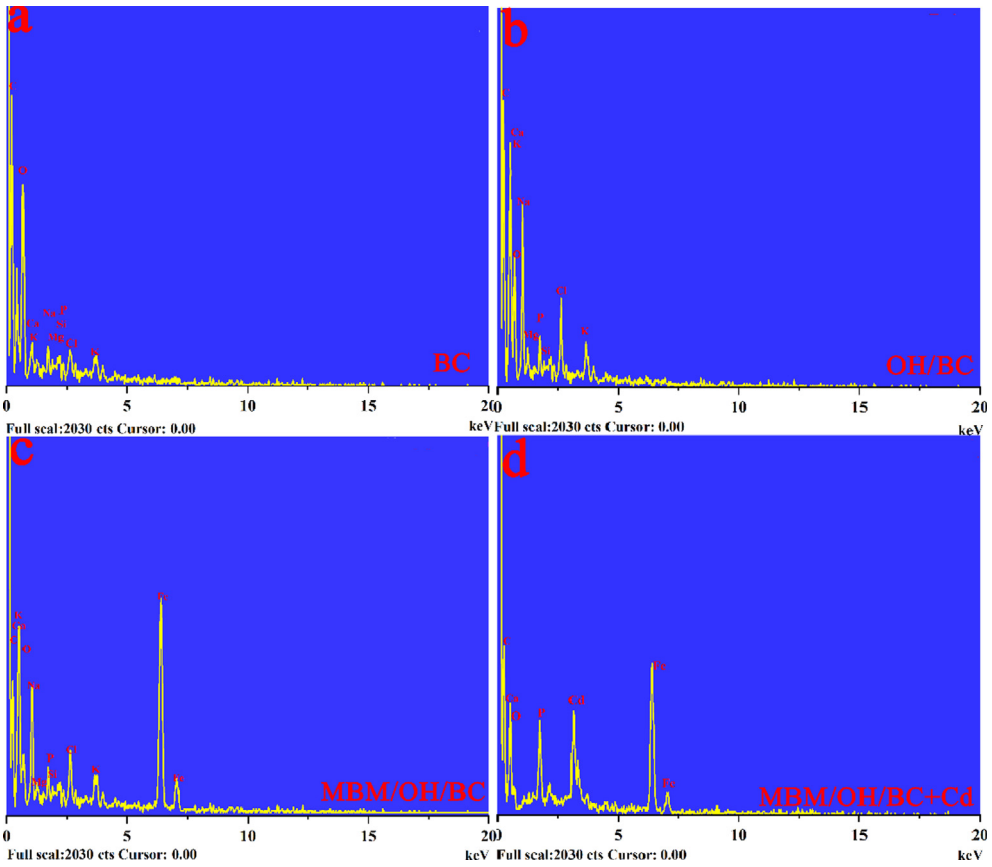

Fig. 12 (a-c) The EDS spectra image analysis of BC, OH/BC and MBM/OH/BC. (d) The EDS spectra image analysis of MBM/OH/BC after Cd^{2+} adsorption.

OH/BC presented the 3D network structure (Fig. 5b). Compared with BC (Fig. 5a), OH/BC presented a larger specific surface area, which could significantly increase the contact and action area with heavy metal ions, thereby promoting the adsorption efficiency for heavy metal ions. In Fig. 5c, it could be clearly seen that there were lots of spherical particles attached to the surface and inside of the biochar, which was considered as Fe_3O_4, which could be further proved by SEM-mapping. The spectrum of SEM mapping showed that Fe elements were evenly distributed in MBM/OH/BC (Fig. 9). The above results confirmed that Fe_3O_4 particles were successfully extruded onto the biochar adsorbent by ball-milling. Meanwhile, the VSM was used to study its magnetic performance. The hysteresis curves showed the saturation magnetization of MBM/OH/BC was 37.09 emu/g and all magnetic biochar materials were strongly attracted to an external magnet (Fig. 9d), which implied that it was enough to be magnetically separated from the solution under an external magnetic field, and it was conducive to the recycling and reuse of adsorbent materials.

3.4.4. NaOH and ball-milling modification effect on specific surface area

The BET surface area and pore volume values for the BC, OH/BC and MBM/OH/BC were obtained from the N_2 adsorption or desorption isotherms. According to Fig. S5a, BC, OH/BC and MBM/OH/BC showed a typical IV type curve in accordance with the IUPAC (International Union of Pure and Applied Chemistry) and the type H_4 hysteresis loop was observed, which indicated that those adsorbents had lots of microporous structures and occurred the phenomenon of capillary condensation (Feng, et al., 2021; Zhou, et al., 2018). This result was further proved by the pore diameter distribute curves (Fig. S6b). In addition, the detailed data of the BET surface area and pore volume values were shown in Table 4. From Table 4, it could be found that the specific surface area and pore volume of the biochar adsorbent were significantly increased after NaOH and ball-milling modification, and the specific surface area has increased from 64.45 to 148.41 m^2/g^{-1}, and the pore volume has increased from 0.091 to 0.178 cm^3/g^{-1}, which was consistent with the results of SEM

Table 4 The textural properties of BC, OH/BC and MBM/OH/BC.

Textural properties	BC	OH/BC	MBM/OH/BC
S_{BET} – surface area (m^2 g^{-1})	64.45	288.91	148.41
V_T – total pore volume (cm^3 g^{-1})	0.091	0.315	0.178
D_p – average pore diameter (nm)	4.153	3.061	1.985

and it could enhance the adsorption and removal ability for heavy metals ions.

3.5. Desorption and regeneration

The magnetic MBM/OH/BC could be easily separated from the aqueous solution with an external magnetic field, so it was convenient to recycle and reuse. In four adsorption and desorption cycles, the adsorption capacity of MBM/OH/BC was 136.2 mg/g, 128.4 mg/g, 117.5 mg/g and 109.0 mg/g, respectively (Fig. S7), which indicated that MBM/OH/BC had excellent reproducibility and reusability.

3.6. Comparison with other biochar adsorbents

The comparison with other biochar adsorbents used for the removal of Cd^{2+} was summarized in Table S1. It could be found that the adsorption capacity of MBM/OH/BC to Cd^{2+} was significantly higher than other adsorbents, which further proved that the NaOH and ball-milling modification could significantly improve the adsorption capacity of biochar. Meanwhile, the MBM/OH/BC also had a high adsorption rate and reusability.

4. Conclusions

This study synthesized a high adsorption performance, recyclable magnetic nano-carbon material by facile NaOH and ball-milling co-modifying biochar. The results showed MBM/OH/BC exhibited excellent adsorption capacity, high adsorption efficiency and good reusability at the same time. In addition, in order to explain its adsorption mechanism in-depth, the qualitative and quantitative mechanisms were investigated. The adsorption process could be well described by the pseudo-second-order kinetic model (R^2 = 0.994) and Freundlich isotherm model (R^2 = 0.997), indicating the adsorption process was mainly controlled by chemisorption. The results of XRD, SEM-EDS, FTIR, XPS, Raman and DFT calculation showed that the mechanisms of MBM/OH/BC adsorbing Cd^{2+} mainly include physical adsorption, cation exchange, precipitation, complexation and coordination. Meanwhile, according to the result of quantitative mechanisms, the precipitation, cation exchange and complexation were the primary adsorption mechanism, which jointly contributed 90% of the total adsorption. Therefore, it could be concluded that NaOH and ball-milling modification was a powerful modification method to improve the adsorption capacity of biochar for heavy metals ions. In the follow-up research, we will further explore the interaction and influence mechanism of ions in their binary ion system, ternary ion system and multi-component ion system.

Acknowledgements

This work is supported by Sichuan Provincial Administration of Traditional Chinese Medicine: Study on the adsorption efficiency and mechanism of the heavy metal cadmium in Ligusticum chuanxiong by the magnetic biomass nano-carbon porous material based on the waste residue of traditional Chinese medicine (No. 2021MS022). Sichuan Provincial Department of Science and Technology Application Basic Project: Research on Rapid Detection Technology of Sulfur Dioxide Limit based on Baizhi Scientific Sulphur Fumigation Technology (No. 2020YJ0369).

Appendix A. Supplementary material

Supplementary data to this article can be found online at https://doi.org/10.1016/j.arabjc.2022.103817.

References

Aichour, A. et al, 2022. Highly removal of anionic dye from aqueous medium using a promising biochar derived from date palm petioles: characterization, adsorption properties and reuse studies. Arab. J. Chem. 15 (1).

Baharum, N.A. et al, 2020. Highly efficient removal of diazinon pesticide from aqueous solutions by using coconut shell-modified biochar. Arab. J. Chem. 13 (7), 6106–6121.

Chen, H. et al, 2021. Sorption of diethyl phthalate and cadmium by pig carcass and green waste-derived biochars under single and binary systems. Environ. Res 193, 110594.

Chen, Q. et al, 2019. A multi-functional-group modified cellulose for enhanced heavy metal cadmium adsorption: performance and quantum chemical mechanism. Chemosphere 224, 509–518.

Chen, Y. et al, 2020. Novel magnetic pomelo peel biochar for enhancing Pb(II) And Cu(II) adsorption: performance and mechanism. Water Air Soil Pollut. 231 (8).

Cheng, S., et al. 2021a. Lead and cadmium clean removal from wastewater by sustainable biochar derived from poplar saw dust. J. Clean. Product. 314.

Cheng, S., et al., 2021b. Efficient and selective removal of Pb(II) from aqueous solution by modification crofton weed: experiment and density functional theory calculation, J. Clean. Product. 280.

Cheng, S. et al, 2022. High-efficiency removal of lead/cadmium from wastewater by MgO modified biochar derived from crofton weed. Bioresour. Technol. 343, 126081.

Ding, Z. et al, 2016. Removal of lead, copper, cadmium, zinc, and nickel from aqueous solutions by alkali-modified biochar: batch and column tests. J. Ind. Eng. Chem. 33, 239–245.

Du, H. et al, 2021. Multifunctional magnetic bio-nanoporous carbon material based on zero-valent iron, Angelicae Dahuricae Radix slag and graphene oxide: an efficient adsorbent of pesticides. Arabian J. Chem. 14 (8).

Feng, D. et al, 2021. Functionalized construction of biochar with hierarchical pore structures and surface O-/N-containing groups for phenol adsorption. Chem. Eng. J. 410.

Fernando, J.C. et al, 2021. Nitric acid surface pre-modification of novel Lasia spinosa biochar for enhanced methylene blue remediation. Groundwater Sustain. Dev. 14.

Fu, C. et al, 2021. Study of adsorption property and mechanism of lead(II) and cadmium(II) onto sulfhydryl modified attapulgite. Arabian J. Chem. 14 (2).

Fu, J. et al, 2013. Influence of e-waste dismantling and its regulations: temporal trend, spatial distribution of heavy metals in rice grains, and its potential health risk. Environ. Sci. Technol. 47 (13), 7437–7445.

Gao, L.Y. et al, 2019. Relative distribution of Cd(2+) adsorption mechanisms on biochars derived from rice straw and sewage sludge. Bioresour. Technol. 272, 114–122.

Glicklich, D. et al, 2020. Heavy metal toxicity in chronic renal failure and cardiovascular disease: possible role for chelation therapy. Cardiol. Rev. 28 (6), 312–318.

Guo, Z. et al, 2017. Biomass-derived carbon sorbents for Cd(II) removal: activation and adsorption mechanism. ACS Sustain. Chem. Eng. 5 (5), 4103–4109.
Han, Z. et al, 2015. Magnetite impregnation effects on the sorbent properties of activated carbons and biochars. Water Res. 70, 394–403.
Herath, A. et al, 2021. KOH-activated high surface area douglas fir biochar for adsorbing aqueous Cr(VI), Pb(II) and Cd(II). Chemosphere 269, 128409.
Hosseini, H. et al, 2021. Removal of methylene blue from wastewater using ternary nanocomposite aerogel systems: carboxymethyl cellulose grafted by polyacrylic acid and decorated with graphene oxide. J. Hazard. Mater. 421, 126752.
Hu, X. et al, 2015. Batch and column sorption of arsenic onto iron-impregnated biochar synthesized through hydrolysis. Water Res. 68, 206–216.
Huang, F. et al, 2018. Quantitative contribution of Cd(2 +) adsorption mechanisms by chicken-manure-derived biochars. Environ. Sci. Pollut. Res. Int. 25 (28), 28322–28334.
Huang, F. et al, 2020. Qualitative and quantitative characterization of adsorption mechanisms for Cd(2 +) by silicon-rich biochar. Sci. Total Environ. 731, 139163.
Islam, M.S. et al, 2021. Biochar heavy metal removal in aqueous solution depends on feedstock type and pyrolysis purging gas. Environ. Pollut. 281, 117094.
Johri, N. et al, 2010. Heavy metal poisoning: the effects of cadmium on the kidney. Biometals 23 (5), 783–792.
Li, Y. et al, 2018. Qualitative and quantitative correlation of physicochemical characteristics and lead sorption behaviors of crop residue-derived chars. Bioresour. Technol. 270, 545–553.
Li, Y. et al, 2020. Solvent-free synthesis of magnetic biochar and activated carbon through ball-mill extrusion with Fe_3O_4 nanoparticles for enhancing adsorption of methylene blue. Sci. Total Environ. 722, 137972.
Liu, L. et al, 2020. Investigating the adsorption behavior and quantitative contribution of Pb(2 +) adsorption mechanisms on biochars by different feedstocks from a fluidized bed pyrolysis system. Environ. Res. 187, 109609.
Liu, Y. et al, 2021. A new nanocomposite assembled with metal organic framework and magnetic biochar derived from pomelo peels: a highly efficient adsorbent for ketamine in wastewater. J. Environ. Chem. Eng. 9 (5).
Lyu, H. et al, 2018a. Effects of ball milling on the physicochemical and sorptive properties of biochar: experimental observations and governing mechanisms. Environ. Pollut. 233, 54–63.
Lyu, H. et al, 2018b. Experimental and modeling investigations of ball-milled biochar for the removal of aqueous methylene blue. Chem. Eng. J. 335, 110–119.
Lyu, H. et al, 2020. Thiol-modified biochar synthesized by a facile ball-milling method for enhanced sorption of inorganic Hg(2 +) and organic CH3Hg(.). J. Hazard Mater. 384, 121357.
Munera-Echeverri, J.L. et al, 2018. Cation exchange capacity of biochar: an urgent method modification. Sci. Total Environ. 642, 190–197.
Qiu, B. et al, 2021. Biochar as a low-cost adsorbent for aqueous heavy metal removal: a review. J. Anal. Appl. Pyrol. 155.
Romero-González, J. et al, 2005. Determination of thermodynamic parameters of Cr(VI) adsorption from aqueous solution onto Agave lechuguilla biomass. J. Chem. Thermodyn. 37 (4), 343–347.
Sari, A. et al, 2007. Adsorption characteristics of Cu(II) and Pb(II) onto expanded perlite from aqueous solution. J. Hazard Mater. 148 (1–2), 387–394.
Shan, D. et al, 2016. Preparation of ultrafine magnetic biochar and activated carbon for pharmaceutical adsorption and subsequent degradation by ball milling. J. Hazard Mater. 305, 156–163.
Sun, Y. et al, 2019. Multifunctional iron-biochar composites for the removal of potentially toxic elements, inherent cations, and hetero-chloride from hydraulic fracturing wastewater. Environ. Int. 124, 521–532.
Tang, Y. et al, 2021. Removal of emerging contaminants (bisphenol A and antibiotics) from kitchen wastewater by alkali-modified biochar. Sci. Total Environ. 805, 150158.
Thines, K.R. et al, 2017. Synthesis of magnetic biochar from agricultural waste biomass to enhancing route for waste water and polymer application: a review. Renew. Sustain. Energy Rev. 67, 257–276.
Wang, K. et al, 2020. Aqueous Cr(VI) removal by a novel ball milled Fe(0)-biochar composite: role of biochar electron transfer capacity under high pyrolysis temperature. Chemosphere 241, 125044.
Wang, L. et al, 2019. Mechanisms and reutilization of modified biochar used for removal of heavy metals from wastewater: a review. Sci. Total Environ. 668, 1298–1309.
Wang, T. et al, 2021. Adsorption and visible-light photocatalytic degradation of organic pollutants by functionalized biochar: Role of iodine doping and reactive species. Environ. Res. 197, 111026.
Xiao, Y. et al, 2020. Effects of ball milling on the photochemistry of biochar: Enrofloxacin degradation and possible mechanisms. Chem. Eng. J. 384.
Xu, Y. et al, 2016. Enhanced adsorption of methylene blue by citric acid modification of biochar derived from water hyacinth (Eichornia crassipes). Environ. Sci. Pollut. Res. Int. 23 (23), 23606–23618.
Yang, J. et al, 2021. Efficient recovery of phosphate from aqueous solution using biochar derived from co-pyrolysis of sewage sludge with eggshell. J. Environ. Chem. Eng. 9 (5).
Yu, W. et al, 2018. N-doping effectively enhances the adsorption capacity of biochar for heavy metal ions from aqueous solution. Chemosphere 193, 8–16.
Yu, Y. et al, 2020. Unraveling sorption of Cr (VI) from aqueous solution by FeCl3 and ZnCl2-modified corn stalks biochar: Implicit mechanism and application. Bioresour. Technol. 297, 122466.
Zhang, H. et al, 2021a. Adsorption of two beta-blocker pollutants on modified montmorillonite with environment-friendly cationic surfactant containing amide group: batch adsorption experiments and Multiwfn wave function analysis. J. Colloid Interface Sci. 590, 601–613.
Zhang, M. et al, 2013. Preparation and characterization of a novel magnetic biochar for arsenic removal. Bioresour. Technol. 130, 457–462.
Zhang, P. et al, 2021b. Characteristics, adsorption behaviors, Cu(II) adsorption mechanisms by cow manure biochar derived at various pyrolysis temperatures. Bioresour. Technol. 331, 125013.
Zhang, Q. et al, 2019a. Ball-milled biochar for galaxolide removal: sorption performance and governing mechanisms. Sci. Total Environ. 659, 1537–1545.
Zhang, S. et al, 2019b. Magnetic apple pomace biochar: Simple preparation, characterization, and application for enriching Ag(I) in effluents. Sci. Total Environ. 668, 115–123.
Zhou, H. et al, 2022. Sodium citrate and biochar synergistic improvement of nanoscale zero-valent iron composite for the removal of chromium (VI) in aqueous solutions. J. Environ. Sci. 115, 227–239.
Zhou, K. et al, 2020a. Waste biomass-derived oxygen and nitrogen co-doped porous carbon/MgO composites as superior acetone adsorbent: experimental and DFT study on the adsorption behavior. Chem. Eng. J. 387.
Zhou, Y. et al, 2018. Controllable synthesis of magnetic nanoporous carbon with tunable porosity for the efficient cleanup of vegetable samples. Anal. Chim Acta 1041, 58–67.
Zhou, Y. et al, 2020b. A three dimension magnetic bio-char composite-based quick, easy, cheap, effective, rugged and safe method for multi-pesticides analysis of vegetables. J. Chromatogr A 1615, 460770.

Zhu, S. et al, 2020. Rapid removal of toxic metals Cu2 + and Pb2 + by amino trimethylene phosphonic acid intercalated layered double hydroxide: a combined experimental and DFT study. Chem. Eng. J. 392.

Zhuang, Z. et al, 2021. Efficient removal of volatile organic compound by ball-milled biochars from different preparing conditions. J. Hazard. Mater. 406, 124676.

Zoroufchi Benis, K. et al, 2020. Treatment of aqueous arsenic – a review of biochar modification methods. Sci. Total Environ. 739, 139750.

Zubair, M. et al, 2021. Sustainable wastewater treatment by biochar/layered double hydroxide composites: progress, challenges, and outlook. Bioresour. Technol. 319, 124128.